Energy Relaxation Dynamics of Photofragments Measured by Probe Beam Deflection Technique: Photodissociation of CF_3I at 266 nm

Myungkoo Suh, Wookyung Sung, Seong-Ung Heo, and Hyun Jin Hwang*

Department of Chemistry, Kyung Hee University, Seoul 130-701, Korea

Received: June 16, 1999; In Final Form: August 16, 1999

Energy relaxation dynamics of photofragments produced from photodissociation of trifluoromethyl iodide (CF_3I) in argon at 266 nm was studied by means of a time-resolved probe beam deflection (PBD) technique. It was found that the PBD transients observed in Ar environment consist of two heat-releasing (via collisional relaxation) processes that can be assigned to translational-to-translational (T−T) and vibrational-to-translational (V−T) energy transfers of photofragments. From the relaxation times and the fractions of the two processes, 15% of the excess energy from photodissociation was found to be partitioned into vibrational modes of CF_3 radicals while the remaining 85% goes to translation. In additon, the intermolecular V−T energy-transfer rate constant between CF_3 and Ar was determined to be $\sim 8.0 \times 10^2$ s^{-1} $Torr^{-1}$. Electronic to translational (E−T) energy transfer from the spin−orbit excited iodine fragment, $I^*(^2P_{1/2})$, to the medium was not observed in the time domain employed in this study, unless oxygen, a well-known I* quencher, was added to facilitate the transfer process. An excellent agreement between the obtained results and previously reported photofragment translational spectroscopy results indicates that the energy relaxation processes of photofragments as well as energy partitioning of excess energy can be studied by the PBD method presented in this study.

Introduction

The dynamics of energy transfer during and after photodissociation plays important roles in photochemical and photophysical processes. Consequently, it has been a subject of many studies.[1−6] When photodissociation is taking place, the excess energy over the bond dissociation energy is distributed into translational, rotational, vibrational, and electronic modes of photofragments. The energy partitioning into those modes depends on the nature of potential energy surfaces involved.[1,2] Following the photodissociation, energies deposited into different modes of photofragments equilibrate with the medium, i.e., surrounding molecules or atoms, via intermolecular collisions. This results in an increase of the translational energy, i.e., temperature, of the medium. Depending on the nature of photofragment energy levels, the energy transfer from photofragments to the medium occurs on different time scales; for example, rotational-to-translational (R−T) and translational-to-translational (T−T) energy transfers happen much faster than vibrational-to-translational (V−T) and electronic-to-translational (E−T) energy transfers. Therefore, studies of the collisional relaxation dynamics of photofragments can provide information on various intermolecular energy-transfer processes of photofragments as well as the energy partitioning during photodissociation.

To study intermolecular energy transfers, various time-resolved methods have been utilized to monitor the energy-transfer processes in the time domain. Among the methods, photothermal techniques such as thermal lensing and probe beam deflection have been applied for numerous energy-transfer studies successfully.[7−16] In contrast to optical methods such as transient absorption[17] and time-resolved emission[18] techniques, which monitor the fate of relaxing molecules directly, photothermal methods monitor the transient heat deposition to the medium that gives rise to the time-dependent change in the refractive index of the medium. Therefore, photothermal methods can be applied to the systems where the optical transient monitoring is not feasible because of the inherent nature of the molecules of interest. Processes with a wide range of relaxation time, from microseconds to milliseconds, can be studied simply by adjusting experimental parameters such as excitation beam parameter and/or concentrations of chemical species involved in the process. Despite the wide applicability of photothermal methods, only a few energy relaxation processes of radicals have been studied by using the methods. The V−T energy-transfer process of a stable radical NO_2 was studied with the thermal lensing technique.[7] Also very recently, we reported the V−T energy-transfer process of a phenyl radical produced from photodissociation of iodobenzene by using the same method with an improved time resolution.[19]

In the present study, the relaxation dynamics of photofragments produced from photodissociation of trifluoromethyl iodide (CF_3I) at 266 nm was studied by means of a probe beam deflection method. CF_3I was selected because the UV photodissociation of CF_3I has been well characterized by photofragment translational spectroscopy (PTS) studies.[20−22] Upon excitation in its first UV absorption band, CF_3I undergoes a prompt C−I bond dissociation via one of two energetically distinct reaction channels:

$$CF_3I + h\nu \rightarrow CF_3 + I(^2P_{3/2}) \quad (1)$$

$$CF_3I + h\nu \rightarrow CF_3 + I^*(^2P_{1/2}) \quad (2)$$

In a recent PTS study of CF_3I at 248 nm,[22] Felder reported that the branching ratio of channel 1 to channel 2 is 0.11:0.89, indicating a preferential production of spin−orbit excited iodine atoms, $I^*(^2P_{1/2})$. In addition to the branching ratio, partitioning

* To whom correspondence should be addressed. Phone: 82-2-961-0298. Fax: 82-2-966-3701. E-mail: hjhwang@nms.kyunghee.ac.kr.

10.1021/jp991969g CCC: $18.00
Published on Web 10/04/1999

of excess energy into translational and internal energies of the photofragments was also well characterized. Generally, when the relaxation dynamics of photofragments are monitored, the high reactivity of photofragments could complicate the photothermal measurement by releasing thermal energies upon chemical reactions, such as radical recombinations. However, the radical recombination reactions of CF_3I photofragments are known[23] to be much slower than the collisional energy relaxation processes we are interested in. Therefore, the energy relaxation processes observed in CF_3I photodissociation can be readily interpreted in terms of relaxation dynamics of photofragments.

In this paper, a probe beam deflection (PBD) method with a modified crossed-laser-beam geometry was utilized in order to investigate the relaxation process of photofragments produced from photodissociation of CF_3I at 266 nm. By analyzing the time-resolved PBD signals, we determined the excess energy partitioning between various modes of photofragments as well as their relaxation rates. The results were compared with the energy partitioning of CF_3I photofragments measured by the PTS method[22] and V−T and E−T transfer rates of chemical species reported previously.[7,24,25] Apart from its simplicity, the PBD method provided results similar to the ones measured by highly sophisticated methods such as PTS, inferring its applicability to the study of the dynamics of energy transfer during and after the photodissociation.

Experiments

Trifluoromethyl iodide, 99% purity, was purchased from Aldrich Chemical Co., Inc. (Milwaukee, WI) and used without further purification. High-purity oxygen (99.99%) and argon (99.9999%) were purchased from Dongjin Jonghab Gas Co. (Seoul, Korea). Argon was used after passing through an oxygen scrubber from J&W Scientific, Inc. (Folsom, CA) in order to remove trace oxygen.

The whole gas-sampling apparatus, including the sample cell, gas inlet lines, connectors, and valves, was made of stainless steel to avoid possible corrosion by photofragment radicals. The sample cell equipped with quartz windows was a 304 stainless steel block (58 mm × 58 mm × 140 mm) that had two through-holes perpendicular to each other for irradiation of pump and probe laser beams (a 30 mm i.d. × 140 mm hole for the pump beam and a 18 mm i.d. × 58 mm hole for the probe beam). The sample cell and the gas lines were flushed with Ar gas at least three times before introducing new sample gases. Absolute pressures of the sample gases were measured by a capacitance manometer (MKS model 122AA-01000AD). All experiments were performed at ambient temperature (22 °C).

The optical setup for monitoring probe beam deflection signals is schematically depicted in Figure 1. The pump beam was a 266 nm pulsed laser that was the fourth harmonic of a Q-switched Nd:YAG laser (Spectra Physics, GCR-150) with ∼5 ns pulse width and ∼9 mm beam diameter. The pulse energy of the pump laser beam was kept low enough (300 μJ/pulse) to avoid complications due to multiphoton absorption processes. The probe beam was a 632.8 nm CW He−Ne laser (Uniphase model 1125P) with ∼1 mm beam diameter and 5 mW output power. As shown in Figure 1, the excitation pump beam and the probe beam were aligned to be crossed at the center of the sample cell (not shown) with a perpendicular geometry. A spherical converging lens ($f = 100$ mm) was used to focus the probe beam to the center of the sample cell. To enhance the interaction length of the two beams, the pump beam was line-focused into the sample cell so that its long axis was aligned

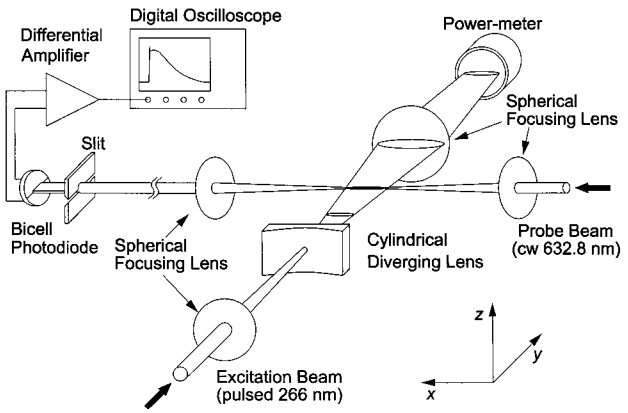

Figure 1. Experimental setup for photothermal beam deflection studies. The probe beam crosses the excitation beam inside the stainless steel sample cell equipped with quartz windows, which is omitted for clarity.

along the probe beam propagating direction. Combination of a spherical converging lens ($f = 250$ mm) and a cylindrical diverging lens ($f = -75$ mm) was used to shape the pump beam into a line of ∼140 μm × 30 mm at the region where the probe beam crossed the pump beam. In this optical arrangement, the intensity distribution of the pump laser along the *x*- and *y*-directions can be assumed to be nearly uniform compared to that along the *z*-direction. The vertical intensity distribution of the pump beam along the *z*-axis is described by $I = I_0 \exp(-2z^2/w_0^2)$ where w_0 is $1/e^2$ Gaussian beam radius. The value of w_0 was 70 ± 5 μm under typical experimental conditions. For the probe beam deflection measurements, the probe beam was positioned at $z = 40 \pm 5$ μm with respect to the center of the line-focused pump beam. The probe beam deflection signal, caused by the time-dependent change of the refractive index in the pump−probe interaction region, was monitored by a bicell photodiode detector (UDT model SPOT-9DMI) equipped with a *z*-discrimination slit with an 800 μm opening. The bicell detector was located at a distance of 140 cm from the pump−probe interaction region, and the probe beam was refocused to ∼4 mm diameter at the detector by using a 250 mm focal length spherical lens. By use of the *z*-discrimination slit, the effective beam radius of the probe beam can be reduced, and therefore, a slight enhancement of sensitivity and time resolution can be achieved. The PBD signal was amplified with a home-built differential amplifier (×100 gain, 20 MHz bandwidth) and recorded by a digital oscilloscope (LeCroy model 9460). The overall detector response time measured with a ∼5 ns laser pulse was ∼40 ns. The digitized signals were transferred to a personal computer for further analysis.

Theory

A brief description of the theory and the resulting equations describing time-dependent PBD signals will be given here. We followed the treatment given by Tam,[12,13] and its detailed discussions can be found in references therein. Suppose an excitation beam and a probe beam are propagating along the *y*- and *x*-directions, respectively (see Figure 1). The excitation beam that is focused by a spherical focusing lens with a focal length *f* to have a Gaussian beam waist w_0 is expanded to a length *l* in the *x*-direction by a cylindrical diverging lens. Since *l* and *f* are much greater than w_0, we can assume that the intensity distribution of the excitation light in the *z*-direction is Gaussian with a beam parameter w_0, while those in the *x*- and *y*-directions are uniform. Therefore, heat flows to *x*- and *y*-directions can be neglected compared to that along the *z*-direction.

When a weakly absorbing sample is exposed to a short excitation pulse, the temperature rise due to a pulsed heat source Q is described by

$$T(z,t) = \int_0^t dt' \int_{-\infty}^{\infty} dz'\, G(z',z,t-t')\, Q(z',t') \qquad (3)$$

where Green's function $G(z',z,t-t')$ is

$$G(z',z,t-t') = \frac{\exp[-(z-z')^2/(4D(t-t'))]}{2\sqrt{\pi D(t-t')}} \qquad (4)$$

and heat source term $Q(z',t')$ is

$$Q(z',t') = N(z',t')\, h\nu \frac{\exp(-t'/\tau)}{\tau}$$
$$= \frac{\sqrt{2}\alpha E_0 \exp[-2z'^2/(w_0^2 + 8D_m t')]}{\rho C_p \sqrt{\pi}\tau\sqrt{w_0^2 + 8D_m t'}} \exp\left(-\frac{t'}{\tau}\right) \qquad (5)$$

Here, $N(z',t')$ is the concentration of the excited molecules. D is the thermal diffusivity of the medium, D_m is the molecular diffusivity, E_0 is the pump beam energy, and α is the optical absorption coefficient. $h\nu$ is the excitation photon energy, ρ is the density, C_p is the specific heat at constant pressure, and τ is the thermal relaxation time. In eq 5, it is assumed that the heat-releasing process can be described by a single relaxation time τ. Integrating eq 3 yields

$$T(z,t) = \frac{\sqrt{2}\alpha E_0}{\sqrt{\pi}\rho C_p \tau} \int_0^t \frac{\exp(-t'/\tau)}{\sqrt{A(t,t')}} \exp\left(-\frac{2z^2}{A(t,t')}\right) dt' \qquad (6)$$

where

$$A(t,t') = w_0^2 + 8D_m t' + 8D(t-t')$$

In a crossed-beam setup, the time-dependent probe beam deflection in the z-direction ϕ is described by

$$\phi(t,z) = \frac{1}{n}\frac{\partial n}{\partial T}\int_{-\infty}^{\infty} \frac{\partial T}{\partial z}\, dx \qquad (7)$$

where n is the refractive index. When the relaxation of the excited molecule is faster than the thermal and mass diffusion, or else $D_m \approx D$, which is the case for most gas-phase systems, the time-dependent probe beam deflection can be solved by substituting eq 6 into eq 7:

$$\phi(t,z) = \frac{1}{n}\frac{\partial n}{\partial T}\frac{(-8\alpha E_0 z l)}{\sqrt{2\pi}\rho C_p}\frac{[1-\exp(-t/\tau)]}{(w_0^2 + 8Dt)^{1.5}} \exp\left(-\frac{2z^2}{w_0^2 + 8Dt}\right) \qquad (8)$$

where z is the probe beam position with respect to the center of the excitation beam.

It should be noted that the eq 8 is valid only if the probe beam is much narrower than the pump beam, since the probe beam is approximated to a single ray. When the probe beam has a beam waist, w_p, that is comparable to that of the excitation beam, w_0, the observed probe beam deflection becomes the average deflection of each ray consisting of the probe beam. Spatial integration of the probe beam intensity profile over the expression given as eq 8 results in the average deflection as shown by Bialkowski and He:[26]

$$\langle\phi(t,z_0)\rangle = \frac{\sqrt{2}}{w_p\sqrt{\pi}}\int_{-\infty}^{\infty}\phi(t,z)\exp[-2(z-z_0)^2/w_p^2]\, dz$$
$$= \frac{1}{n}\frac{\partial n}{\partial T}\frac{(-8\alpha E_0 z_0 l)}{\pi\rho C_p}\frac{[1-\exp(-t/\tau)]}{(w_{app}^2 + 8Dt)^{1.5}} \times \exp\left(-\frac{2z_0^2}{w_{app}^2 + 8Dt}\right) \qquad (9)$$

where z_0 is the separation between the centers of the pump and probe lasers and w_{app} is the combined beam waist, which is equal to $(w_0^2 + w_p^2)^{1/2}$ for Gaussian shaped pump and probe beams. Note that the maximum deflection occurs at $z_0 = \pm(1/2)w_{app}$. The time dependence of the PBD signal described in eq 9 is quite different from eq 8 as shown in Figure 2. The dotted curve in Figure 2 is simulated on the basis of eq 9, and the solid curve is based on eq 8 when $w_0 = w_p = 60$ μm and $\tau = 10$ μs. When two curves are compared, the PBD decay of a finite volume probe beam is more diffused than the PBD decay based on ray approximation. This suggests that the combined beam waist w_{app} must be measured in situ as done in this work by directly measuring the z dependence of the PBD signal (see Figure 3).

If two heat-releasing processes are involved and furthermore if they are well separated in time, i.e., one process relaxes much faster than the other, the time-dependent PBD signal can be

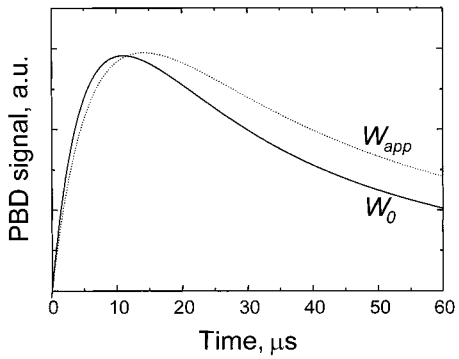

Figure 2. Theoretical PBD curves calculated by approximating the probe beam as a single ray (solid line) and as a beam with a finite volume (dotted line). w_0, w_p, and τ are set to 60 μm, 60 μm, and 10 μs, respectively.

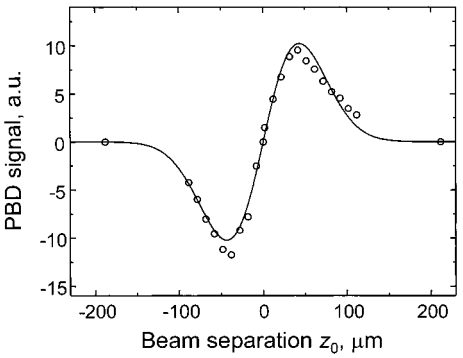

Figure 3. Typical plot of peak intensities of the PBD signals at various pump and probe beam separations. Open circles represent experimental data, and the solid line is the nonlinear least-squares fitting result using eq 10 at a constant time. From this curve w_{app} is estimated to be 84 $\pm$1 μm.

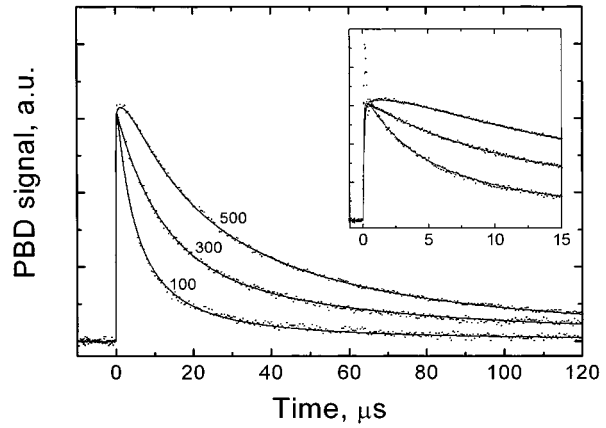

Figure 4. PBD transients for CF_3I and Ar mixtures at various total pressures. The solid and dotted lines represent the fitting results and experimental data, respectively. The partial pressure of CF_3I was 0.40 Torr, and the total pressures (in Torr) are indicated with curves. The inset displays early time behavior where a slow heat-releasing process is clearly observed as a plateau when total pressure reaches 500 Torr.

described with two relaxation times:

$$\langle\phi(t,z_0)\rangle = \frac{1}{n}\frac{\partial n}{\partial T} \times \frac{(-8\alpha E_0 z_0 l)}{\pi\rho C_p}\frac{[1 - r_1\exp(-t/\tau_1) - (1 - r_1)\exp(-t/\tau_2)]}{(w_{app}^2 + 8Dt)^{1.5}} \times \exp\left(-\frac{2z_0^2}{w_{app}^2 + 8Dt}\right) \quad (10)$$

τ_1 and r_1 are the relaxation time and the fraction of the fast process, respectively, while τ_2 and r_2 are the ones for the slow process.

To determine the relaxation times and the fractions of the two relaxation processes by fitting the experimental PBD transient with the derived equation, it is important to measure the w_{app} and z_0 values accurately. In the present study, z_0 was determined by reading a micrometer attached to a vertical translational stage on which the excitation beam assembly is mounted. Determination of z_0 was guided by the fact that the PBD signal vanishes at $z_0 = 0$ according to eqs 9 and 10. Uncertainties in z_0 was estimated to be a few micrometers in the present setup. The apparent beam parameter along *z*-axis, w_{app}, was determined by monitoring the PBD signal intensity as a function of z_0. Figure 3 shows how the intensity of the probe beam deflection signal changes with respect to the relative position of the probe beam, z_0. The w_{app} value was determined by a nonlinear fitting of the peak intensities of PBD signals with eq 10. From the fitting, w_{app} was determined to be 84 ± 1 μm. Since the pump beam parameters are critical for obtaining reliable kinetic information, they were monitored constantly throughout the experiments.

Results

The PBD signals at various total pressures are depicted in Figure 4. After the photodissociation of CF_3I, the resulting thermal energy released to the medium by intermolecular energy transfer decays mainly by thermal diffusion. As the argon pressure increases, the signal decay slows, since the thermal diffusivity is inversely proportional to the pressure. As the pressure reaches ~500 Torr, a slower heat release process becomes distinct, as shown by the small plateau at early times (see Figure 4 inset). The observed signals were fitted with eqs 9 and 10 described in the previous section. When the argon pressure was relatively low, ≤400 Torr, the transient PBD signals were fitted very well with a single rise time 0.2 μs as τ. However, when the argon pressure was ~500 Torr, the fitting attempt with a single rise time failed. Instead, the given experimental PBD transient was fitted successfully with two heat release components: 0.20 and 2.5 μs for τ_1 and τ_2, respectively. As shown in Figure 4, there is excellent agreement between the PBD signal and the derived equations. The thermal diffusivity, *D*, as well as τ and *r* were obtained from the fitting.

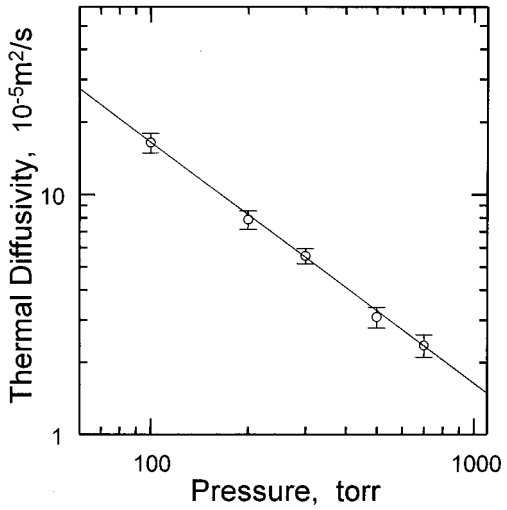

Figure 5. Thermal diffusivity values for various total pressures. Open circles are determined by fitting experimental data. Solid line represents the calculated values. The error bars represent 1σ values obtained from multiple measurements. For calculations, only the contribution from argon gas was considered.

It should be noted that the τ_1 value, 0.20 μs, was chosen on the basis of the time resolution of our experimental setup. In general, the time resolution of the PBD experiment is governed by the acoustic transit time, τ_a, of the initial photothermal acoustic wave across the pump beam. τ_a is described as $\tau_a = w_0/s$, where w_0 is the beam parameter of the pump laser and *s* is the speed of sound in the medium. With our typical optical arrangement, the τ_a value was ~0.20 μs. Since the acoustic rise time was ~0.1 μs and the detector response time measured with a short laser pulse was 40 ns, the time resolution of our experimental system was limited by the acoustic transit time. Various τ_1 values from 10 ns to 0.30 μs were tried for the fitting and showed no appreciable difference in the fitting results. We, therefore, chose 0.20 μs as the τ_1 value for our convenience.

The thermal diffusivity values estimated from the fitting were compared with the theoretical values calculated by using $D = \lambda/(\rho C_p)$, where λ is the heat conductivity, ρ is the density, and C_p is the specific heat at constant pressure. In Figure 5, the thermal diffusivity values from the measured experimental PBD signals (open circles) are plotted with the calculated ones (solid line) at various total pressures. An excellent agreement between the experimental results and the theoretical values strongly indicates that the derived equations describe the observed time-resolved PBD signals correctly.

The PBD transient signals obtained for photodissociation of CF_3I in 500 Torr of Ar at various excitation laser powers are shown in Figure 6. Normalized signals are completely indistinguishable at the excitation power range we tested. As mentioned in Figure 4, the PBD signals at 500 Torr of Ar fit well with two heat-release processes with the relaxation times 0.20 μs and 2.5 ± 0.8 μs. We also changed the partial pressure of CF_3I up to 1 Torr and found the same results. The fractional

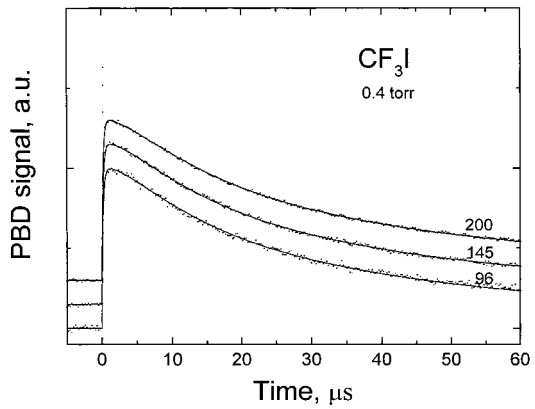

Figure 6. PBD transients for CF_3I and Ar mixture at various excitation laser powers. The solid lines correspond to the best fits (see Table 1 for fitting parameters). All curves were normalized, and their baselines were displaced for clarity. The excitation powers (in μJ/pulse) are indicated with the curves. CF_3I pressure was 0.40 Torr, and the total pressure was adjusted to 500 Torr with Ar.

contribution of the slow component was determined to be 0.15 $\pm$ 0.02 (see Table 1 for the fitting summary). Possible thermal-energy-releasing processes after the photodissociation of CF_3I are T−T, V−T, R−T, and E−T energy transfers and recombination reactions of photofragments. In the present study, concentrations of photofragment radicals, CF_3 and I, were kept low ($\leq 4 \times 10^{-3}$ Torr) in order to suppress the radical combination reactions. With the given radical concentrations, it is estimated that the recombination reactions among them take place on the millisecond time scale,[23,27] which is too slow to be detected in the present experimental setup. For gas-phase species (at atmospheric pressure and at room temperature), T−T and R−T energy transfers as well as V−V and R−R energy transfers are known to occur on a time scale of molecular collisions,[28,29] ca. $10^{-8}-10^{-10}$ s, which is much faster than the acoustic transit time of 0.20 μs. On the other hand, V−T transfer falls into the microsecond time scale for most polyatomic molecules in the gas phase under similar experimental conditions.[28,30] Therefore, it is reasonable to attribute the observed fast energy-releasing process to T−T and R−T energy transfers and the slow one with a 2.5 μs relaxation time to V−T energy transfer of CF_3. Note that E−T transfer of the spin−orbit excited $I^*(^2P_{1/2})$ atoms is known to occur on a much longer time scale under the given experimental conditions.[31] The r_2 value was determined to be 0.15 $\pm$ 0.02, indicating that about 15% of the available energy of photofragments is distributed to the vibrational energy of CF_3. Since the V−T transfer rate will depend on the vibrational energy, the observed relaxation time must be considered as an average relaxation time from different vibrational states.

Iodine atoms at a spin−orbit excited $I^*(^2P_{1/2})$ state was reported to undergo radiationless electronic transition on a microsecond time scale in the presence of a small amount of effective I* quenchers (say, for example, less than 1 Torr of O_2).[31] To investigate the contribution from the electronic energy of I*, a well-known I* quencher O_2 (0.5 Torr) was added to the CF_3I systems and their PBD signals were monitored (see Figure 7). Again, the normalized curves are identical to each other regardless of the laser power, indicating lack of dependence on the excitation laser power. The PBD transient curves fit well with two relaxation times, and the fitting results are summarized in Table 1. By addition of O_2 to a CF_3I and Ar mixture, the contribution of the slow heat-releasing process increased from 15% to 56%, and its relaxation time slowed to 10.6 $\pm$ 1.7 μs. An interesting fitting parameter is the A_0 value, which is proportional to the total heat released. In addition, the A_0r_1 value is proportional to the amount of heat released from the fast relaxation process while A_0r_2 is proportional to that from the slow relaxation process. When A_0 values are compared in the presence and in the absence of O_2, the A_0r_1 value remains constant while A_0r_2 increases 7.4 times upon the addition of O_2. The additional relaxation process that contributes to the increase in A_0r_2 can be attributed mostly to I* quenching by oxygen molecules. The PBD signals depending on the excitation laser power are plotted in Figure 8. For both cases, the slope of the log−log plot is 1.1 $\pm$ 0.1, indicating that the heat relaxation processes result from one-photon absorption of CF_3I, which leads to a prompt breakage of the C−I bond.

Discussion

In the present study, we found that 15% of the available energy is partitioned into vibrational energy during photodissociation of CF_3I at 266 nm while the remaining 85% is partitioned into translation. This vibrational energy can be compared with the average internal energy of photofragments determined by photofragment translational spectroscopy (PTS). Although no PTS study of CF_3I photodissociated at 266 nm has been carried out, we can estimate the energy partitioning at 266 nm by using the PTS results at 248 [22] and 275 nm.[32] It was suggested by both theory[20,33] and experiments[32,34] that the internal energy of CF_3 decreases almost linearly as excitation photon energy decreases for both I and I* channels. We, therefore, estimated energy partitioning at 266 nm by assuming a linear dependence of the CF_3 internal excitation on the photon energy between 248 and 275 nm and assuming that the I* quantum yield at 266 nm is the same as that measured at 248 nm ($\phi^* = 0.89$). As summarized in Table 2, the average translational, internal, and electronic energies of CF_3I photofragments at 266 nm are estimated to be 26.2, 6.7, and 19.3 kcal/mol, respectively. From this estimation, $\langle E_t \rangle$:$\langle E_{r,v} \rangle$ is calculated to be 0.80:0.20, which indicates that 20% of available energy is distributed as internal energy during photodissociation at 266 nm. This estimated internal energy fraction agrees well with the vibrational energy of photofragments obtained by the present PBD method (15% of the available energy). The small difference is likely due to the fact that the value of $\langle E_{r,v} \rangle$ estimated from the PTS results contains a small contribution from the rotational energy of CF_3. It is also possible that a part of the V−T energy transfer from high vibrational states, whose relaxation time is shorter than the acoustic transit time, is excluded from the average vibrational energy obtained by the present PBD method. However, the small difference as estimated above suggests that most of the V−T energy transfer of CF_3 radicals takes place on a time scale that is longer than the acoustic transit time.

The observed V−T energy-transfer process seems to occur between CF_3 radicals and argon atoms, since we observed that τ_2 depended on argon pressures but not on either CF_3I pressure or photodissociation laser powers. Unfortunately, the reliable argon pressure dependence of τ_2 could not be measured in this study, since at higher argon pressures the relaxation times fall too close to the acoustic transit time. Nevertheless, from the observed relaxation time, 2.5 μs measured at 500 Torr of argon, the average V−T energy-transfer rate constant from CF_3 radicals to Ar atoms was approximated to be 8.0×10^2 s^{-1} $Torr^{-1}$. It is worthwhile to note that the observed V−T energy transfer is from well-defined vibrational states of CF_3. The vibrational excitation of CF_3 during the photodissociation of CF_3I in the A band is known to be confined almost exclusively in the $\nu_2(a_2')$ umbrella bending mode (703 cm^{-1}).[22] The average vibrational

TABLE 1: Summary of Fitting Results[a]

sample composition (Torr)							
CF_3I[b]	O_2	Ar	r_1	r_2	τ_1 (μs)	τ_2 (μs)	A_0 (AU)
0.40	0	500	0.85(0.02)	0.15(0.02)	0.20	2.5(0.8)	1.00(0.13)
0.40	0.50	500	0.44(0.04)	0.56(0.04)	0.20	10.6(1.7)	1.99(0.23)

[a] Equation 10 was used for the fitting to determine r_1, r_2, τ_2, and A_0. Note that A_0 is proportional to the total thermal energy released, and it is equal to $(1/n)(\partial n/\partial T)[-8\alpha E_0 z_0 l/(\pi\rho C_p)]$ in eq 10. The values of w_{app} and z_0 (84 ± 5 μm and 40 ± 5 μm, respectively) were obtained from experimental measurements, and the value of the thermal diffusivity D (3.2×10^{-5} m^2 s^{-1}) was calculated from the equation $D = \lambda/(\rho C_p)$. The value of τ_1 was taken to be the acoustic transit time. Varying the τ_1 value from 50 to 300 ns had no significant effect on the fitting results. Numbers in parentheses are 1σ values of the fitting results obtained from multiple measurements. [b] We also attained the same fitting results when the partial pressure of CF_3I was 0.70 and 1.0 Torr.

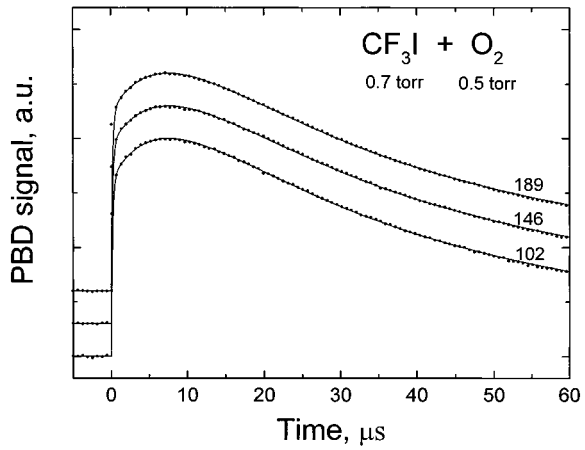

Figure 7. PBD transients for CF_3I and Ar mixture in the presence of oxygen molecules at various excitation laser powers. The solid lines correspond to the best fits (see Table 1 for fitting parameters). All curves were normalized, and their baselines were displaced for clarity. The excitation powers (in μJ/pulse) are indicated with the curves. CF_3I and O_2 pressures were 0.70 and 0.50 Torr, respectively. Total pressure was adjusted to 500 Torr with Ar.

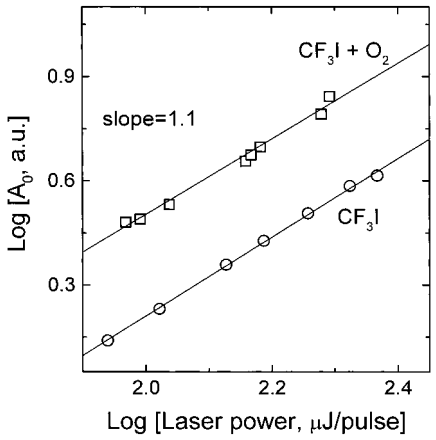

Figure 8. Amount of total released heat observed in PBD transient, A_0, as a function of excitation laser powers. Open squares and circles represent A_0 values in the presence and in the absence of O_2, respectively. CF_3I and O_2 pressures were 0.40 and 0.50 Torr, respectively. Total pressure was adjusted to 500 Torr with Ar.

energy of CF_3 radicals at 266 nm, which is estimated from 15% of the available energy, is 4.9 kcal/mol ($\sim$1700 cm^{-1}). This average vibrational energy corresponds to $\sim$2.5 quanta of the umbrella bending vibration on average.

Since the V−T energy transfer rate depends on the vibrational state of the chemical species, it would be relevant to compare the V−T rate constant of CF_3 to Ar obtained in the present study with those of the molecules excited to low-lying vibrational levels. We found that the observed V−T transfer rate constant of CF_3 to Ar obtained in the PBD study, 8.0×10^2 s^{-1} Torr^{-1}, is similar to the ones of several molecules excited to low vibrational levels. For example, the V−T rate constant of C_2H_4 to Ar when C_2H_4 was pumped to the ν_7 (949.2 cm^{-1}) vibrational mode was reported as 4.7×10^2 s^{-1} Torr^{-1},[24] and that of CCl_2F_2 excited to the ν_6 (922 cm^{-1}) mode was 8.6×10^3 s^{-1} Torr^{-1}.[30] Also, the V−T transfer rate constant of a stable radical NO_2 to argon, in which NO_2 is in the (010) state, was reported as 1.8×10^3 s^{-1} Torr^{-1}.[7] This similarity in the V−T energy-transfer rate constants is consistent with the finding that the observed slow heat-releasing process in the present PBD study results from V−T energy transfer.

TABLE 2: Energy Partitioning (in kcal/mol) in the Photodissociation of CF_3I[a]

wavelength (nm)	$\langle E_t \rangle$ (kcal/mol)	$\langle E_{r,v} \rangle$ (kcal/mol)	$\langle E_e \rangle$ (kcal/mol)	ϕ^*	note
248	31.0	11.4	19.3	0.89	ref 22
275	26.5	4.3	19.9	0.917	ref 32
266	26.2	6.7	19.3	0.89	estimated[b]
266	28.0	4.9			this work[c]

[a] The energy partitioning values are weighted-average values of the $I(^2P_{3/2})$ and $I^*(^2P_{1/2})$ channels by using the quantum yield of I* (ϕ^*). The bond dissociation energy is taken to be the revised value of Felder ($D_0^0 = 55.2$ kcal/mol).[35] [b] Estimated by using the PTS data at 248 [22] and 275 nm[32] assuming that internal excitation of CF_3 radicals depends linearly on the excitation photon energy for each of the I and I* channels. The ϕ^* value is assumed to be the same as that at 248 nm. [c] Calculated by using the r_2 value observed in the absence of O_2 and assuming $\phi^* = 0.89$. In the absence of O_2, $\langle E_{r,v} \rangle$ corresponds to 15% of the sum of $\langle E_t \rangle$ and $\langle E_{r,v} \rangle$. See text for details.

The average energy transferred per collision, $\langle \Delta E \rangle$, for the observed V−T transfer of CF_3 to argon can be estimated by the following relationship:

$$\langle \Delta E \rangle = \frac{\langle E_v \rangle (1 - e^{-1})}{Z_{CF_3-Ar}\tau} \qquad (11)$$

where τ is the observed V−T relaxation time, $\langle E_v \rangle$ is the total vibrational energy, and $\langle E_v \rangle (1 - e^{-1})$ is the vibrational energy transferred during the time period τ. Z_{CF_3-Ar} is the collision frequency between CF_3 and 500 Torr of Ar. $\langle E_v \rangle$ is 1700 cm^{-1}, and τ is 2.5 μs. Assuming Z_{CF_3-Ar} is similar to Z_{CF_3I-Ar}, 4.9×10^9 s^{-1},[36] $\langle \Delta E \rangle$ is estimated to be $\sim$0.090 cm^{-1}. This inefficient energy transfer is typical for V−T transfer processes of small molecules at low vibrational levels in the gas phase. For example, $\langle \Delta E \rangle$ for the V−T transfer of NO_2 (010) to Ar is estimated to be $\sim$0.077 cm^{-1} according to eq 11.[7] Also, on the basis of the result reported previously,[37] $\langle \Delta E \rangle$ for the V−T transfer of OCS(001) to Ar is estimated as $\sim$0.046 cm^{-1}.

In the presence of oxygen molecules, the slow energy-releasing process became dominated by I* quenching by oxygen molecules. Consequently, the total energy released as thermal energy in the presence of oxygen molecules was twice the one in the absence of oxygen mainly because of the additional

energy contribution from I* quenching. Our PBD finding indicates that 56% of the energy transfer in a thermal form originated from the slow energy-releasing processes. The energy released from this slow process in the presence of O_2 corresponds to the sum of the internal energy of CF_3 and the electronic energy of I*. By use of the estimated PTS results at 266 nm shown in Table 2, $\langle E_t\rangle$:$\langle E_e\rangle + \langle E_{r,v}\rangle$ is calculated to be 0.50:0.50, which indicates that the fraction of the slow energy-releasing process is 50%. Therefore, there is a discrepancy, 6% of the available energy corresponding to ca. 3.1 kcal/mol, between our PBD result and the PTS result. This discrepancy may suggest the possible existence of other heat-releasing process(es). The reactions between CF_3 radicals and oxygen molecules seem to be the plausible reactions to account for the discrepancy. It is known that the CF_3 radical reacts with O_2 to form CF_3O_2 followed by fast multistep reactions to produce CF_2O as a final product.[38,39] The rate constant for the formation of CF_3O_2 is reported as 1.40×10^5 s^{-1} $Torr^{-1}$.[38] Since the reported rate constant of I* quenching by oxygen molecules[25] is 8.8×10^5 s^{-1} $Torr^{-1}$, it is likely that a part of the thermal energy observed in the PBD experiment is due to the reactions between CF_3 radicals and oxygen molecules.

It is interesting to note that the observed rate constant that is calculated from τ_2 in the presence of oxygen, 1.9×10^5 s^{-1} $Torr^{-1}$, is smaller than the rate constant of I* quenching by oxygen molecules reported previously, 8.8×10^5 s^{-1} $Torr^{-1}$, which is measured by time-resolved atomic absorption from I*. Although the observed τ_2 value is an apparent relaxation time comprising of at least three relaxation processes, still the value reflects mainly I* quenching process by oxygen molecules, since it is a major process. The difference in rate constants is due to the difference in the experimental methods employed. In the PBD method, the time evolution of the thermal energy released to the medium was measured but not the evolution of I* itself. I* quenching by oxygen molecules and the subsequent thermal energy transfer to argon takes place in the following order:

$$CF_3I + h\nu \rightarrow CF_3 + I^* \quad (12)$$

$$I^* + O_2 \rightarrow O_2^{\ddagger} + I \quad (13)$$

$$O_2^{\ddagger} + M \rightarrow O_2 + M \quad (14)$$

where $O_2^{\ddagger}$ denotes vibrationally and rotationally excited O_2 molecules and M denotes various surrounding gas molecules in the medium. The PBD method measures the combined rate of reactions 13 and 14, while the atomic absorption measurement follows reaction 13. By comparing the two rate constants, it can be concluded that reaction 14 is slower than reaction 13 and consequently becomes the rate-determining step. Vibrational deactivation of O_2 by Ar is reported to be 8−9 orders of magnitude slower[40] than the rate constant observed in the present experiment. This suggests that the deactivation of $O_2^{\ddagger}$ most likely occurs via collisions with other molecular species in the medium such as O_2, CF_3I, and CF_3.

In summary, we have shown that the PBD method presented in this study provides a versatile experimental method for investigating various collisional energy relaxation processes of photofragments. By studying the time dependence of heat-releasing processes of photofragments produced from photodissociation, we were able to determine energy partitioning of excess energies into various energy modes during photodissociation as well as V−T energy-transfer rates of photofragments. Simultaneous monitoring of both the energy partitioning and the energy-transfer rate provides a unique opportunity to study collisional vibrational relaxation of radical species with well-defined vibrational energies.

Acknowledgment. This work was supported by the Specified Basic Research Fund of the Korea Science and Engineering Foundation (KOSEF 94-0501-02-05-3) and in part by the Hallym Academy of Sciences, Hallym University. M.S. acknowledges the postdoctoral support from Kyung Hee University.

References and Notes

(1) Wodtke, A. M.; Lee, Y. T. *Molecular Photodissociation Dynamics*; Ashfold, M. N. R., Baggott, J. E., Eds.; Royal Society of Chemistry: London, 1987; p 31.

(2) Leone, S. R. *Adv. Chem. Phys.* **1982**, *50*, 255.

(3) Grimley, A. J.; Houston, P. L. *J. Chem. Phys.* **1978**, *68*, 3366.

(4) Johnson, B. R.; Kittrell, C.; Kelly, P. B.; Kinsey, J. L. *J. Phys. Chem.* **1996**, *100*, 7743.

(5) Butler, L. J.; Neumark, D. M. *J. Phys. Chem.* **1996**, *100*, 12801.

(6) Braslavsky, S. E.; Heibel, G. E. *Chem. Rev.* **1992**, *92*, 1381.

(7) Toselli, B. M.; Walunas, T. L.; Barker, J. R. *J. Chem. Phys.* **1990**, *92*, 4793.

(8) Barker, J. R.; Toselli, B. M. *Photothermal Investigations of Solids and Fluids*; Academic: New York, 1989; Chapter 5.

(9) Franko, M.; Tran, C. D. *Rev. Sci. Instrum.* **1996**, *67*, 1.

(10) Grabiner, F. R.; Siebert, D. R.; Flynn, G. W. *Chem. Phys. Lett.* **1972**, *17*, 189.

(11) Bialkowski, S. E. *Photothermal Spectroscopy Methods for Chemical Analysis*; Wiley, New York, 1996; Vol. 134.

(12) Tam, A. C. *Photothermal Investigations of Solids and Fluids*; Academic: New York, 1989; Chapter 1.

(13) Sontag, H.; Tam, A. C.; Hess, P. *J. Chem. Phys.* **1987**, *86*, 3950.

(14) Poston, P. E.; Harris, J. M. *J. Am. Chem. Soc.* **1990**, *112*, 644.

(15) Calasso, I. G.; Delgadillo, I.; Sigrist, M. W. *Chem. Phys.* **1998**, *229*, 181.

(16) Laman, D. M.; Falvey, D. E. *Rev. Sci. Instrum.* **1996**, *67*, 3260.

(17) Hippler, H.; Lindemann, L.; Troe, J. *J. Chem. Phys.* **1985**, *83*, 3906.

(18) Barker, J. R.; Toselli, B. M. *Int. Rev. Phys. Chem.* **1993**, *12*, 305.

(19) Lee, J. S.; Hwang, H. J. *Bull. Korean Chem. Soc.* **1997**, *18*, 11.

(20) van Veen, G. N. A.; Baller, T.; de Vries, A. E.; Shapiro, M. *Chem. Phys.* **1985**, *93*, 277.

(21) Felder, P. *Chem. Phys.* **1990**, *143*, 141.

(22) Felder, P. *Chem. Phys.* **1991**, *155*, 435.

(23) Vakhtin, A. B. *Int. J. Chem. Kinet.* **1996**, *28*, 443.

(24) Yuan, R. C. L.; Flynn, G. W. *J. Chem. Phys.* **1973**, *58*, 649.

(25) Burde, D. H.; McFarlane, R. A. *J. Chem. Phys.* **1976**, *64*, 1850.

(26) Bialkowski, S. E.; He, Z. F. *Anal. Chem.* **1988**, *60*, 2674.

(27) Burde, D. H.; McFarlane, R. A.; Wiesenfeld, J. R. *Chem. Phys. Lett.* **1975**, *32*, 296.

(28) Flygare, W. H. *Acc. Chem. Res.* **1968**, *1*, 121.

(29) Flygare, W. H. *Molecular Structure and Dynamics*; Prentice Hall: Englewood Cliffs, NJ, 1978.

(30) Xing-Xiao, M.; Zhu-De, X. *Chem. Phys. Lett.* **1983**, *98*, 563.

(31) Donovan, R. J.; Husain, D. *Chem. Rev.* **1970**, *70*, 491.

(32) Furlan, A.; Gejo, T.; Huber, J. R. *J. Phys. Chem.* **1996**, *100*, 7956.

(33) Clary, D. C. *J. Chem. Phys.* **1986**, *84*, 4288.

(34) Hwang, H. J.; El-Sayed, M. A. *J. Phys. Chem.* **1992**, *96*, 8728.

(35) Felder, P. *Chem. Phys. Lett.* **1992**, *98*, 563.

(36) Abel, B.; Herzog, B.; Hippler, H.; Troe, J. *J. Chem. Phys.* **1989**, *91*, 900.

(37) Siebert, D. R.; Flynn, G. W. *J. Chem. Phys.* **1976**, *64*, 497.

(38) Kaiser, E. W.; Wallington, T. J.; Hurley, M. D. *Int. J. Chem. Kinet.* **1995**, *27*, 205.

(39) Clemitshaw, K. C.; Sodeau, J. R. *J. Photochem. Photobiol. A.* **1995**, *86*, 9.

(40) Subba Rao, V.; Skinner, G. B. *J. Chem. Phys.* **1984**, *81*, 775.